Single-molecule Magnetoluminescence from a Spatially Confined Persistent Diradical Emitter

Ryota Matsuoka,[1,2*] Shojiro Kimura,[3] Tomoaki Miura,[4] Tadaaki Ikoma,[4] and Tetsuro Kusamoto[1,2,5*]

[1]Department of Life and Coordination-Complex Molecular Science, Institute for Molecular Science, 5-1 Higashiyama, Myodaiji, Okazaki, Aichi 444-8787, Japan

[2]SOKENDAI (The Graduate University for Advanced Studies), Shonan Village, Hayama, 240-0193, Kanagawa, Japan

[3]Institute for Materials Research, Tohoku University, 2-1-1 Katahira, Aoba-ku, Sendai, 980-8577, Japan

[4]Department of Chemistry, Faculty of Science, Niigata University, Niigata, 950-2181, Japan

[5]JST-PRESTO, 4-1-8, Honcho, Kawaguchi, Saitama, 332-0012, Japan.

*Corresponding Authors: Ryota Matsuoka and Tetsuro Kusamoto;
E-mail: matsuoka@ims.ac.jp; kusamoto@ims.ac.jp

Graphical abstract

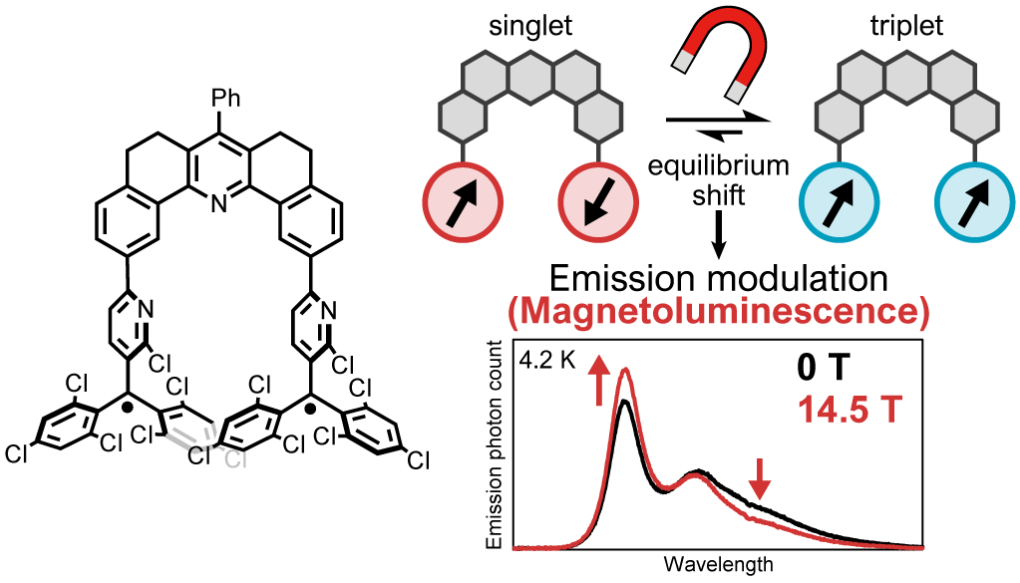

Abstract

Luminescent radicals are an emerging class of materials that exhibit unique photofunctions not found in closed-shell molecules due to their open-shell electronic structure. Particularly promising are photofunctions in which radical's spin and luminescence are correlated; for example, when a magnetic field can affect luminescence (i.e., magnetoluminescence, ML). These photofunctions could be useful in the new science of spin photonics. However, previous observations of ML in radicals have been limited to systems in which radicals are randomly doped in host crystals or polymerized through metal complexation. This study shows that a covalently linked luminescent radical dimer (diradical) can exhibit the ML as a single-molecular property. This facilitates detailed elucidation of the requirements for and mechanisms of ML in radicals and can aid the rational design of ML-active radicals based on synthetic chemistry.

Introduction

Magnetic fields can modulate chemical reactions and materials' properties in a non-contact and non-destructive manner; therefore, they play essential roles in various technologies and biological processes.[1–3] For example, magnetic field effects (MFEs) on electrical resistivity (magnetoresistance) have been applied to magnetic field sensors in computer memories and data storage devices.[2] Magnetic fields are also used to modulate the photophysical and photochemical processes of materials.[1,3–5] Of particular interest are MFEs on molecular luminescence (i.e., magnetoluminescence, ML), which can be used to improve the spatial resolution in optical imaging[6–8] and in the optical monitoring of the yield of singlet oxygen in photodynamic therapy.[9] The ML has also been studied in explorations of the excited-state characteristics of luminescent materials showing exciplex emission,[10–16] delayed fluorescence,[17] phosphorescence,[18,19] triplet–triplet annihilation,[20–24] singlet fission,[25–28] electroluminescence,[29–32] and electrochemiluminescence.[33,34] In these systems, the ML occurs

through the excitation-induced generation of spin-state-correlated species (e.g., radical pairs, polaron pairs, and triplet pairs) with several different spin multiplicities. Applying magnetic fields changes the kinetics of intersystem crossing (ISC) among these spin states and thus the yield of luminescent species generated via spin-dependent pathways.

We previously reported unique ML behavior in persistent open-shell molecules, (3,5-dichloro-4-pyridyl)bis(2,4,6-trichlorophenyl)methyl radical (PyBTM) and its derivatives.[35–41] MFEs were observed when the luminescent radicals were moderately (4–20 wt%) doped into host molecular crystals so that they were partially aggregated (Fig. 1a). Time-resolved emission spectroscopy and quantum mechanical simulations suggested that the MFE is dominated by changes in spin sublevel populations of radical aggregates in the ground states (i.e., before photoexcitation).[40] This contrasts with the MFEs in conventional closed-shell systems described above, which occur only in the transient states produced after excitation. We also recently observed ML from pure solids of one- and two-dimensional coordination polymers containing luminescent radical ligands (Fig. 1b).[42] Their distinct MFE mechanisms give luminescent radicals great promise for developing novel magneto-optical properties that are unachievable by conventional closed-shell luminescent molecules. However, the previous studies were unable to identify the genuine chemical species responsible for the ML of the radicals because they were randomly doped in host crystals or polymerized through metal complexation. Determination of the minimum requirements for the ML of radicals is essential for fully understanding the MFE mechanism, designing novel ML-active radical luminophores, and miniaturizing the ML-active materials ultimately down to the molecular scale for future applications.

Here we report the synthesis, characterization, and photophysical properties of a molecule containing two spatially proximate luminescent radicals (diradical **1**) and the corresponding monoradical (**2**) to elucidate the minimum number of radicals required for ML (Fig. 1c). Photoluminescence behaviors of **2** dispersed well in a polymer matrix were scarcely affected by an applied magnetic field. However, similarly dispersed **1** showed clear changes in its emission characteristics in response to a magnetic field at 4.2 K. This is the first observation of

ML as a single-molecular property in radical compounds. Steady-state and time-resolved luminescence measurements at various temperatures and magnetic fields combined with quantum mechanical simulations indicated that the MFE of **1** originates from a shifting equilibrium among the singlet (S) and triplet (T) ground states and the spin-dependent emission dynamics in the excited states.

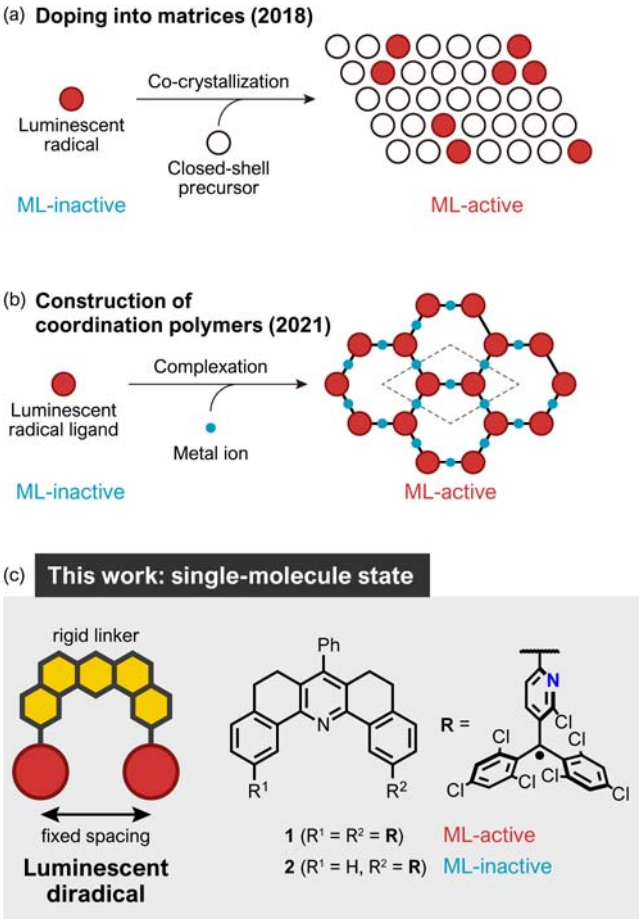

Fig. 1. Schematic illustration of methodologies for achieving ML using luminescent radicals: (a) doping into matrices, (b) construction of coordination polymers (previous studies), and (c) synthesizing a spatially confined diradical as a single-molecule ML-active compound (this study). The chemical structures of luminescent diradical **1** and monoradical **2** investigated here are shown in (c).

Results and Discussion

Molecular design, synthesis, and structural characterization. The diradical **1** consists of two parts: two luminescent (2-chloro-3-pyridyl)bis(2,4,6-trichlorophenyl)methyl radical

moieties linked by a 5,6,8,9-tetrahydro-7-phenyldibenz[*c*,*h*]acridine (THDBA) group. The THDBA linker was chosen for the following features. First, it has a rigid skeleton suitable to confine two luminescent radicals proximal to each other. The spacing provided by the THDBA linker is typically 7–8 Å,[43,44] comparable with the shortest intermolecular radical–radical distances observed in crystals of luminescent polychlorinated triarylmethyl radicals.[39] Second, the two radical–spacer bonds are fixed nearly parallel, forcing the two radical units to adopt similar orientations with respect to the linker. Third, *meta*-connectivity of the aromatic rings in THDBA makes **1** a non-Kekulé diradical, eliminating the contribution of a closed-shell singlet electronic configuration with a quinoid Kekulé structure in the ground state. These characteristics allow the two radical moieties connected by the THDBA linker to interact through space while maintaining their open-shell characters.

The synthesis of the diradical **1** is described in the Supplementary Section 2. The compound was characterized by high-resolution electrospray ionization mass spectrometry and elemental analysis. The presence of two $S = 1/2$ spins was confirmed by quantitative electron spin resonance (ESR) spectroscopy. As a control, a monoradical **2** with one radical moiety attached to THDBA was synthesized using the same starting materials, then characterized similarly to **1**.

The solid-state structure of **1** was determined by single-crystal X-ray diffraction (Fig. 2a,b, and S2). The C1 and C19 atoms adopted an sp^2 hybridized trigonal planar geometry that suggested their radical character. The three aromatic rings around each of these atoms adopted a propeller-shaped conformation, and those around the C1 and C19 atoms showed opposite chirality (one *P* and the other *M*). The linker unit was slightly twisted into a helical shape, and bonded to the pyridine rings of the two radical moieties with torsion angles of 0.2(6)° and 21.9(6)°, respectively. As a result, the radical units were fixed in proximity with a C1···C19 distance of 8.147(5) Å (Fig. 2c). The shortest intramolecular atomic distance between the two radical moieties was 3.013 Å for H12···Cl14, slightly longer than the sum of the van der Waals radii (Fig. S3).

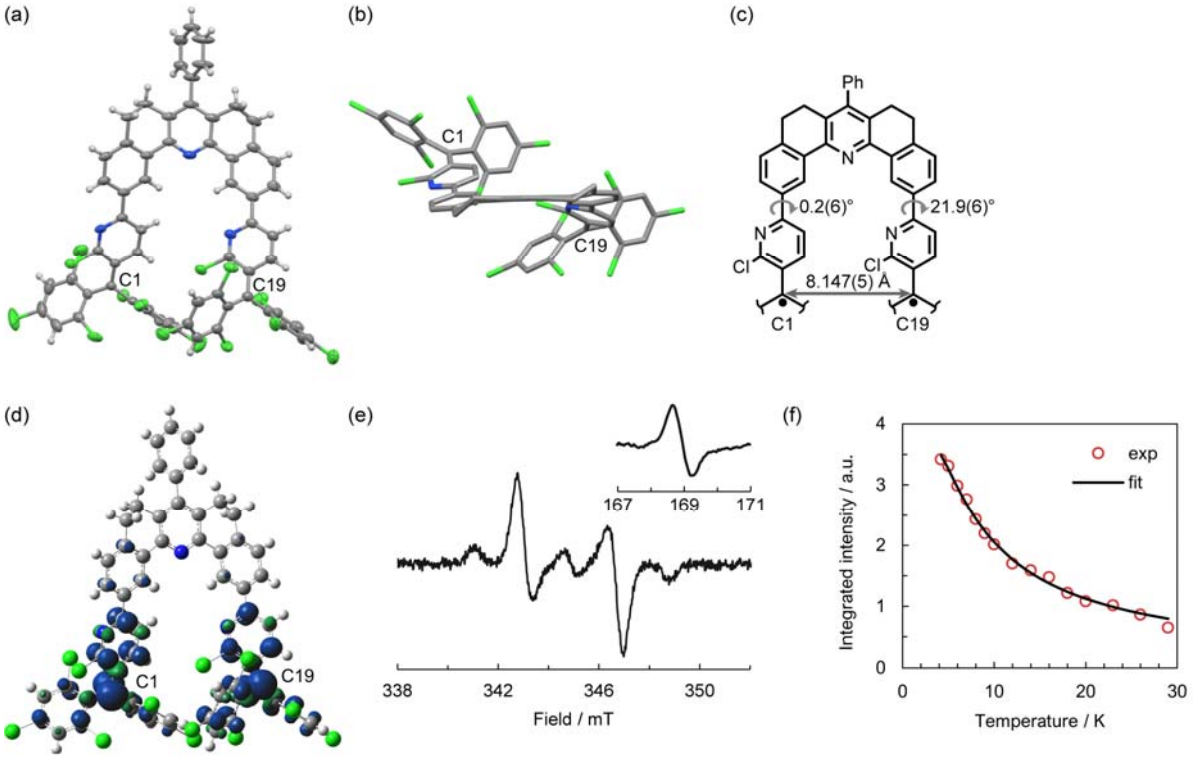

Fig. 2. (a,b) Molecular structure of **1** determined by X-ray crystallography. (a) Ellipsoidal model (50% probability), front view; (b) stick model, side view. Solvent molecules (in (a,b)) and hydrogen atoms (in (b)) are omitted for clarity. (c) Partial chemical structure of **1** showing distance [Å] between the radical centers and dihedral angles [deg] between the linker and the pyridine rings of the radical moieties in the crystal. (d) Spin-density distribution of **1** calculated using DFT (uB3LYP/6-31G(d,p), isovalue = 0.003 a.u.). (e) ESR spectrum of **1** (0.1 wt%) in *α*H-**1** at room temperature. Inset shows the spectrum in the $\Delta m_s = \pm 2$ region at 4.2 K. (f) Temperature dependence of the double integral of the ESR signal intensity for the $\Delta m_s = \pm 2$ forbidden transition of **1** (1 wt%) in PMMA (red circles). The black line represents the theoretical fit according to the Bleaney–Bowers equation.

ESR spectroscopy. The diradical character of **1** was evaluated by solid-state ESR measurements. The ESR spectrum of **1** in poly(methyl methacrylate) (PMMA) at room temperature shows a fine structure signals assignable to triplet diradical species (Fig. S4). More distinct fine structures were observed when **1** was immobilized in crystals of its closed-shell precursor, *α*H-**1** (Fig. S1 shows the crystal structure of *α*H-**1**); there was a typical spectral pattern due to the dipole interaction between the two $S = 1/2$ spins (Fig. 2e). The zero-field splitting parameters estimated from the spectrum are $|D| = 3.85$ mT and $|E| = 0.12$ mT. This $|D|$ value and the point-dipole approximation gave the spin–spin distance as 9.0 Å, reasonably close to the C1···C19 distance (8.15 Å) determined by X-ray structural analysis. Hence, the spin density resided mainly on the two radical moieties, as also suggested by DFT calculations

(UB3LYP/6-31G(d,p)) (Fig. 2d). Half-field signals of forbidden transitions ($\Delta m_s = \pm 2$) were observed at 4.2 K, both in PMMA and in *α*H-**1**, further confirming the triplet character of diradical **1** (Fig. S4 and the inset of Fig. 2e).

Fig. 2f shows the temperature dependence of the signal intensity of the forbidden transitions for **1** in PMMA. Fitting the plot with the Bleaney–Bowers equation[45] estimated the singlet–triplet energy gap ($\Delta E_{S-T} = 2J/k_B$, where J is an exchange coupling constant) to be –5.4 K, indicating a weak antiferromagnetic interaction between the radical moieties. However, broken-symmetry DFT calculations for **1** suggested a weak ferromagnetic interaction with $2J/k_B$ = 1.0 K. This difference in values might arise from the distribution of magnetic interactions in **1** associated with its diverse conformations in PMMA due to the rotation about single bonds between the radical moieties and the linker group.

Photophysical properties at room temperature. Fig. 3a shows the absorption and emission spectra of **1** and **2** in dichloromethane. Both radicals had strong absorption bands at 375 and 430 nm and weak absorption bands at 575 and ~630 nm. The extinction coefficients (ε) of these bands for **1** were about twice as high as those for **2**, indicating that these bands are attributable to excitations involving the radical moiety. The emission spectra of **1** and **2** are almost identical to each other in this condition, suggesting the negligible contribution of radical–radical interactions to this emission band. The photoluminescence quantum yields (ϕ_{em}) of **1** and **2** in dichloromethane were 0.012 and 0.027, respectively, and the respective lifetimes (τ) were 5.5 and 6.9 ns; both properties' values are typical of luminescent triarylmethyl radicals such as PyBTM.[35] In addition, solvent polarity had little effect on the emission wavelength, ϕ_{em}, and τ of **1** and **2** (Tables S1 and S2). This suggests that the radical-centered locally excited character plays a major role in their emissive excited states.

Diradical **1** in a PMMA matrix displayed different emission characteristics from in the solution state: at a concentration of 0.1 wt% in PMMA, its emission band had a similar maximal wavelength (651 nm) to that in dichloromethane (653 nm) but higher relative intensities in the long-wavelength region (>680 nm) (Fig. 3b). Time-resolved emission decay measurements revealed that the emission at 650 nm (hereafter called radical-pair [RP] emission) exhibited a

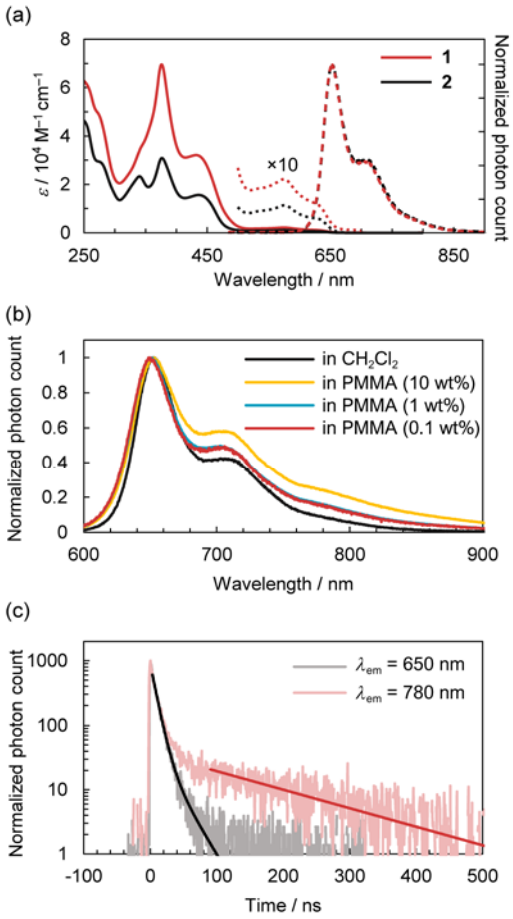

Fig. 3. (a) Absorption (solid lines) and normalized emission (dashed lines, λ_{ex} = 375 nm) spectra of **1** (red) and **2** (black) in CH_2Cl_2 at room temperature. Dotted lines are 10x enlargements of the absorption spectra for λ = 500–700 nm. (b) Normalized emission spectra (λ_{ex} = 375 nm) of **1** in CH_2Cl_2 (black) and PMMA (radical concentration: yellow, 10 wt%; light blue, 1 wt%; red, 0.1 wt%). (c) Emission wavelength dependence of the emission decays of **1** (0.1 wt%) in PMMA at room temperature (λ_{ex} = 375 nm). The black solid line represents theoretical fitting of the decay at λ_{em} = 650 nm by the sum of two exponential functions. The red line represents the theoretical fit of the decay after 100 ns of photoexcitation at λ_{em} = 780 nm using a single-exponential function.

decay behavior analyzed by two components (τ = 8.1 and 25.3 ns), presumably owing to emissions from molecules with various conformations immobilized in PMMA (Fig. 3c). More importantly, an additional decay component with $\tau = 1.5 \times 10^2$ ns was detected at 780 nm, indicating the appearance of a new long-wavelength and long-lasting emission band of **1**. Such a long-lifetime component was not observed for the monoradical **2** at a concentration of 0.2 wt% in PMMA (Fig. S8, S9). Therefore, we attributed this emission to radicals' excimer-like (EX) state intramolecularly generated in **1**. Comparison of the emission of **1** at different concentrations in PMMA revealed that at 0.1 and 1 wt%, **1** showed almost identical emission

spectra, whereas 10 wt% **1** in PMMA showed comparatively enhanced EX emission (Fig. 3b). This enhancement suggests that the higher radical concentration led to the formation of *intermolecular* EX species in addition to the *intramolecular* species. Hence, molecules of **1** dispersed in PMMA are suggested to be well isolated from each other when their concentration is 1 wt% or lower.

Magnetoluminescence. The good dispersibility of **1** in PMMA allows to examine whether two spatially proximate luminescent radical moieties can exhibit ML. Photoluminescence measurements under a magnetic field were conducted for 0.1 wt% **1** and 0.2 wt% **2** (both in PMMA) at cryogenic temperatures. Fig. 4a,b gives the resulting steady-state emission spectra for samples at 4.2 K under magnetic fields of 0, 3, 6, 9, 12, and 14.5 T. The emission of **2** was unaffected by the magnetic field, while the diradical **1** exhibited pronounced MFE in its emission: the intensity of the emission band at 645 nm increased while that at 700–850 nm, seen as a shoulder, decreased with increasing applied field. The single-molecule property of the radical's ML thus appears as the first reported observation of single-molecule ML. At the same time, the minimum number of radicals required for ML is determined to be two (i.e., a radical dimer). The field-induced spectral changes were gradually suppressed as the temperature increased and became almost negligible at 20 K, suggesting that a rising temperature counteracted the MFE (Fig. 4c and S10).

To quantify the field-dependent spectral changes of **1** in PMMA at 4.2 K, the emission spectra were deconvoluted using the time-resolved emission spectra. As the RP and EX emissions of **1** have substantially different lifetimes, we divided the total photon count at each emission wavelength into short-lived ($\leq$ 100 ns) and long-lived ($>>$ 100 ns) components corresponding to RP and EX emission, respectively (Supplementary Section 8 describes the detailed procedure). Superposition of the extracted RP and EX spectral components reproduced well the measured emission spectra (Fig. 4d,e). These fitting results allowed estimation of the contributions of each component (defined as the peak area of each emission band; Fig. 4f). The analysis revealed that the increasing magnetic field simultaneously enhanced the RP emission and suppressed the EX emission. The MFE emerged non-linearly from 1–2 T; it then increased

and leveled off as the field rose to around 12 T, at which the RP emission was enhanced by 22% and the EX emission suppressed by 40%.

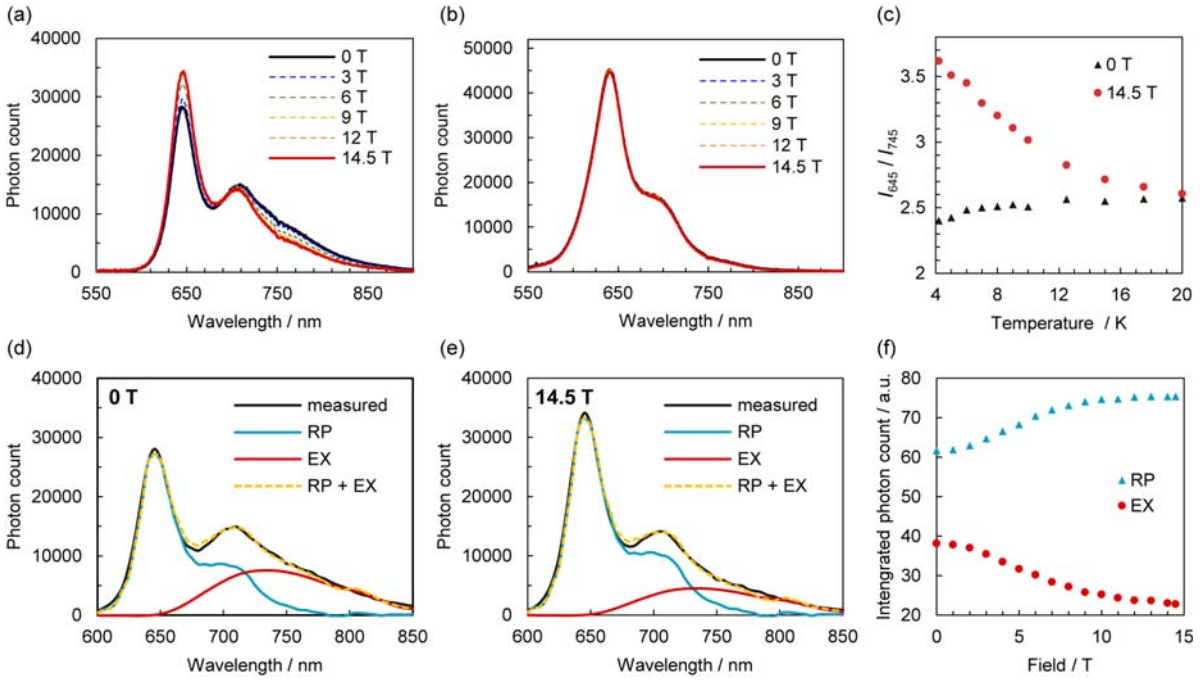

Fig. 4. MFE on radicals' luminescence. Emission spectra of (a) **1** (0.1 wt%) in PMMA and (b) **2** (0.2 wt%) in PMMA at 4.2 K under various magnetic fields. (c) Temperature dependence of the ratio of emission photon counts at 645 and 745 nm (I_{645} / I_{745}) for **1** (0.1 wt%) in PMMA under magnetic fields of 0 and 14.5 T. Deconvolution into the RP and EX emission components of the emission spectra of **1** (0.1 wt%) in PMMA at 4.2 K under magnetic fields of (d) 0 and (e) 14.5 T. (f) Magnetic field dependence of the integrated photon counts of the RP and EX emission components for **1** (0.1 wt%) in PMMA at 4.2 K.

Further information about the MFE was derived from analyzing the emission decay at 650 nm (i.e., the RP emission) (Fig. 5a). Each decay curve collected at different magnetic fields was fitted with the sum of two exponential functions to visualize its changes. Fig. 5b,c summarizes the MFEs on the lifetimes (τ_1, τ_2) and amplitudes (A_1, A_2) at 4.2 K. The lifetimes were almost unaltered by the magnetic field (the averaged τ_1 and τ_2 were 16.8 ± 0.4 ns and 7.0 ± 0.2 ns, respectively), whereas the amplitudes increased significantly with increasing magnetic field. Hence, the enhancement of RP emission under a magnetic field originated from the increased amplitudes. The field-insensitivity of the lifetimes indicated that the magnetic field had little

effect on dynamic processes in the excited state. Rather, the magnetic field statically modulated the proportion of photoexcited species showing RP or EX emissions.

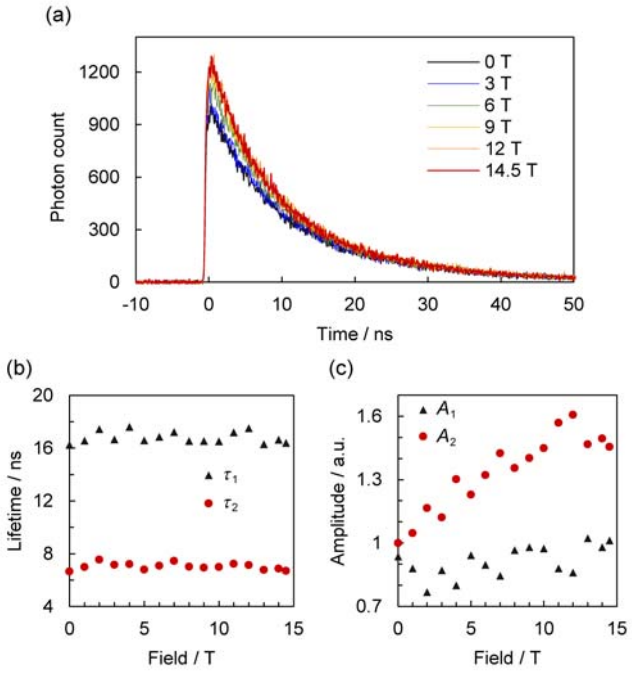

Fig. 5. (a) Decay of emission (λ_{em} = 650 nm) by **1** (0.1 wt%) in PMMA at 4.2 K under various magnetic fields. Magnetic field dependence of (b) lifetimes and (c) amplitudes (λ_{em} = 650 nm) at 4.2 K estimated by fitting the decay curves with the sum of two exponential functions.

MFE mechanisms. From the above observations, we propose the following emission and MFE scheme for **1** (Fig. 6a). Intermolecular interactions between the diradicals were neglected; only intramolecular interactions between the two radical moieties were considered. In the ground state, the diradicals in the singlet (S) and triplet (T_-, T_0, and T_+) states are in thermal equilibrium. Upon photoexcitation at 375 nm, a locally excited RP state is formed conserving the ground-state spin statistics. Both the S- and T-RP states can show RP emission with a rate constant of k_d, but only the S-RP state can generate the S-EX state with a rate constant of k_{EX}, which then shows EX emission. This S-RP → S-EX conversion was expected to be observed as a quick drop of intensity in the initial stage of RP emission decay. However, neither fast decay of the RP emission nor rise of the EX emission was observed under our measurement

conditions (Fig. 3c and 5a). These facts suggest that the S-RP → S-EX conversion was much faster than the instrument response function (~1 ns wide) as well as the radiative and nonradiative decay processes from the S-RP to the ground state.

Under a magnetic field at cryogenic temperature, the equilibrium among the S and T ground states is shifted by Zeeman splitting (Fig. 6a). As the population of the T_- ground state increases and that of the S state decreases with the increasing applied magnetic field, the initial population of the excited T-RP state increases and that of the S-RP state decreases. Thus, the yield of the RP emission increases while that of the EX emission decreases. This MFE on the thermal spin polarization in the ground states is clearly counteracted by rising temperature, which increases the population of higher-energy spin states following the Boltzmann distribution. This MFE is unique to molecules with two or more weakly coupled unpaired electrons in the ground state, where the spin statistics can be easily controlled by magnetic field and temperature. Such MFE is unachievable by luminescent monoradicals and conventional closed-shell molecular luminophores, which possess only one spin multiplicity value in the ground state.

The magnetic field can also accelerate ISC between the S- and T_0-RP excited states through the Δg mechanism, as suggested previously.[40] However, this effect seems negligible in the present system, as evidenced by the lifetimes of the RP emission scarcely varying with the applied magnetic field. Quantum mechanical simulations (Supplementary Section 9) showed significant suppression of MFE because of the Δg mechanism when the S–T_0 energy gap in the RP excited state was much larger than $\Delta g \mu_B B$ (= $0.013 k_B$ K for a difference of the g factor in the two spins, Δg, of 0.0014 and a magnetic field, B, of 14 T). The MFE was also suppressed when S-RP→S-EX conversion (k_{EX}) was significantly faster than $\Delta g \mu_B B/h$ (= 2.8×10^8 s^{-1} for Δg = 0.0014 and B = 14 T). The S-T gap much larger than $\Delta g \mu_B B$ and the fast S-RP→S-EX conversion are possible reasons for the negligible field-dependent ISC of the RP excited state in the present case.

Assuming the excited-state kinetics of **1** is unresponsive to magnetic fields, the field-induced increase of the RP emission amplitudes (A_1 and A_2) should correspond to the increase

of the total populations of the T species (T_{pop}) in the ground state. The field-dependent changes of A_1 and A_2 at 4.2 K estimated using constant lifetimes (τ_1 = 16.8 ns; τ_2 = 7.0 ns) agreed well with the sigmoidal changes of T_{pop} in diradical molecules with J/k_B = 2.3 and –0.6 K, respectively, supporting the proposed MFE mechanism (Fig. 6b). These J values are similar to those estimated from the ESR measurements and DFT calculations. However, the changes in EX emission intensity—which should correspond to changes in the population of S species (S_{pop})—were overestimated using these J values. This implies the presence of singlet diradical species with a negative J value that is so large that the S state population is nearly field-independent up to 14.5 T at 4.2 K. By considering a third species with large negative J (i.e., J/k_B = –20 K), the changes in EX emission intensity were reproduced by the changes of S_{pop} (Fig. 6c). These analyses demonstrate that the observed single-molecule ML behavior can be quantitatively explained by the mechanism shown in Fig. 6a by taking into account the inhomogeneity of J, which is presumably due to the distribution of molecular conformation.

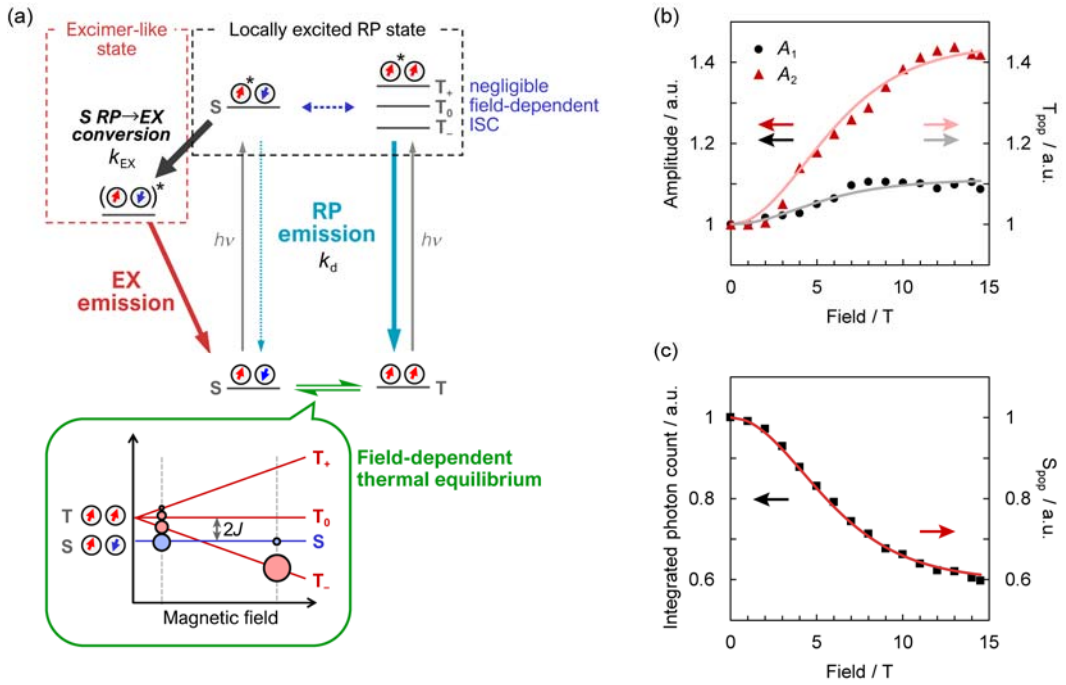

Fig. 6. (a) Proposed scheme for the magnetoluminescence of **1**. (b) Magnetic field dependence of RP emission amplitudes A_1 and A_2 of **1** (λ_{em} = 650 nm) at 4.2 K estimated by fitting the emission decay curves with the sum of two exponential functions using constant lifetimes of τ_1 = 16.8 ns and τ_2 = 7.0 ns. Pink and gray solid lines represent the magnetic field dependence of T_{pop} of diradical molecules with J/k_B = –0.6 and 2.3 K at 4.2 K, respectively. (c) Magnetic field dependence of the integrated photon count for the EX emission of **1** at 4.2 K. The red line represents

the magnetic field dependence of S_{pop} in the presence of diradical molecules with J/k_B = –0.6, 2.3, and –20 K in a 46:29:25 ratio.

Conclusion

We synthesized a spatially confined luminescent radical dimer (**1**) and used steady-state and time-resolved photoemission spectroscopy to explore the fundamental requirements for and mechanisms of its ML under various magnetic fields. At room temperature in PMMA, **1** displayed monomer-like (RP) and intramolecular excimer-like (EX) emissions, the latter being absent from the corresponding monoradical **2**. The intensity ratio of both emissions of **1** in PMMA was modulated by an external magnetic field at temperatures below 20 K. This allowed single-molecule ML in organic radicals to be observed for the first time. The minimum number of radicals required for ML was determined to be two. We attributed the observed MFE to the modulation of the ground-state spin statistics and the spin-dependent excited-state dynamics. This work expands our fundamental understanding of ML in radicals and provides design principles for the ML of radicals at the single-molecular level. The provided molecular design principles will enable the elucidation of (1) more detailed structure–property correlations for the ML of radicals through synthetic structural tuning and (2) deeper insights into excited electronic states and the excited-state dynamics of luminescent diradicals through measurement techniques applicable to solution-like samples (e.g., transient absorption spectroscopy). Both are currently under investigation.

References

1. Steiner, U. E. & Ulrich, T. Magnetic field effects in chemical kinetics and related phenomena. *Chem. Rev.* **89**, 51–147 (1989).
2. Hu, B., Yan, L. & Shao, M. Magnetic-Field Effects in Organic Semiconducting Materials and Devices. *Adv. Mater.* **21**, 1500–1516 (2009).
3. Hore, P. J. & Mouritsen, H. The Radical-Pair Mechanism of Magnetoreception. *Annu. Rev. Biophys.* **45**, 299–344 (2016).
4. Miura, T. Studies on coherent and incoherent spin dynamics that control the magnetic field effect on photogenerated radical pairs. *Mol. Phys.* **118**, e1643510 (2020).
5. Mani, T. Molecular qubits based on photogenerated spin-correlated radical pairs for quantum sensing. *Chem. Phys. Rev.* **3**, 021301 (2022).
6. Lee, H., Yang, N. & Cohen, A. E. Mapping Nanomagnetic Fields Using a Radical Pair Reaction. *Nano Lett.* **11**, 5367–5372 (2011).
7. Yang, N. & Cohen, A. E. Optical imaging through scattering media via magnetically modulated fluorescence: Erratum. *Opt. Express* **19**, 5397 (2011).
8. Le Sage, D. *et al.* Optical magnetic imaging of living cells. *Nature* **496**, 486–489 (2013).
9. Mermut, O. *et al.* The use of magnetic field effects on photosensitizer luminescence as a novel probe for optical monitoring of oxygen in photodynamic therapy. *Phys. Med. Biol.* **54**, 1–16 (2009).
10. Petrov, N. K., Shushin, A. I. & Frankevich, E. L. Solvent effect on magnetic field modulation of excbplex fluorescence in polar solutions. *Chem. Phys. Lett.* **82**, 339–343 (1981).
11. Cao, H. *et al.* Magnetic Field Effects on Intramolecular Exciplex Fluorescence of Chain-Linked Phenanthrene and N , N -Dimethylaniline: Influence of Chain Length, Solvent, and Temperature. *Bull. Chem. Soc. Jpn.* **69**, 2801–2813 (1996).
12. Ito, F., Ikoma, T., Akiyama, K., Kobori, Y. & Tero-Kubota, S. Long-Range Jump versus Stepwise Hops: Magnetic Field Effects on the Charge-Transfer Fluorescence from Photoconductive Polymer Films. *J. Am. Chem. Soc.* **125**, 4722–4723 (2003).
13. Ito, F., Ikoma, T., Akiyama, K., Watanabe, A. & Tero-Kubota, S. Carrier Generation Process on Photoconductive Polymer Films as Studied by Magnetic Field Effects on the Charge-Transfer Fluorescence and Photocurrent. *J. Phys. Chem. B* **110**, 5161–5162 (2006).
14. Kattnig, D. R., Rosspeintner, A. & Grampp, G. Fully Reversible Interconversion between Locally Excited Fluorophore, Exciplex, and Radical Ion Pair Demonstrated by a New Magnetic Field Effect. *Angew. Chem. Int. Ed.* **47**, 960–962 (2008).
15. Richert, S. *et al.* Time-Resolved Magnetic Field Effects Distinguish Loose Ion Pairs from Exciplexes. *J. Am. Chem. Soc.* **135**, 15144–15152 (2013).
16. Kim, D. *et al.* Peptoid-Conjugated Magnetic Field-Sensitive Exciplex System at High and Low Solvent Polarities. *J. Phys. Chem. Lett.* **11**, 4668–4677 (2020).
17. Buck, J. T. & Mani, T. Magnetic Control of Recombination Fluorescence and Tunability by Modulation of Radical Pair Energies in Rigid Donor–Bridge–Acceptor Systems. *J. Am. Chem. Soc.* **142**, 20691–20700 (2020).
18. Takiff, L. & Boxer, S. G. Phosphorescence from the primary electron donor in Rhodobacter sphaeroides and Rhodopseudomonas viridis reaction centers. *Biochim. Biophys. Acta - Bioenerg.* **932**, 325–334 (1988).
19. Mani, T., Tanabe, M., Yamauchi, S., Tkachenko, N. V. & Vinogradov, S. A. Modulation of Visible Room Temperature Phosphorescence by Weak Magnetic Fields. *J. Phys. Chem. Lett.* **3**, 3115–3119 (2012).

20. Johnson, R. C., Merrifield, R. E., Avakian, P. & Flippen, R. B. Effects of Magnetic Fields on the Mutual Annihilation of Triplet Excitons in Molecular Crystals. *Phys. Rev. Lett.* **19**, 285–287 (1967).
21. Merrifield, R. E. Theory of Magnetic Field Effects on the Mutual Annihilation of Triplet Excitons. *J. Chem. Phys.* **48**, 4318–4319 (1968).
22. Faulkner, L. R. & Bard, A. J. Magnetic field effects on anthracene triplet-triplet annihilation in fluid solutions. *J. Am. Chem. Soc.* **91**, 6495–6497 (1969).
23. Mani, T. & Vinogradov, S. A. Magnetic Field Effects on Triplet–Triplet Annihilation in Solutions: Modulation of Visible/NIR Luminescence. *J. Phys. Chem. Lett.* **4**, 2799–2804 (2013).
24. Yokoyama, K. *et al.* Solvent Viscosity Effect on Triplet–Triplet Pair in Triplet Fusion. *J. Phys. Chem. B* **119**, 15901–15908 (2015).
25. Wakasa, M. *et al.* What Can Be Learned from Magnetic Field Effects on Singlet Fission: Role of Exchange Interaction in Excited Triplet Pairs. *J. Phys. Chem. C* **119**, 25840–25844 (2015).
26. Bayliss, S. L. *et al.* Spin signatures of exchange-coupled triplet pairs formed by singlet fission. *Phys. Rev. B* **94**, 045204 (2016).
27. Bayliss, S. L. *et al.* Site-selective measurement of coupled spin pairs in an organic semiconductor. *Proc. Natl. Acad. Sci.* **115**, 5077–5082 (2018).
28. Wang, Z. *et al.* Free-triplet generation with improved efficiency in tetracene oligomers through spatially separated triplet pair states. *Nat. Chem.* **13**, 559–567 (2021).
29. Zhang, Y., Liu, R., Lei, Y. L. & Xiong, Z. H. Low temperature magnetic field effects in Alq3-based organic light emitting diodes. *Appl. Phys. Lett.* **94**, 083307 (2009).
30. Ling, Y. *et al.* Large magneto-conductance and magneto-electroluminescence in exciplex-based organic light-emitting diodes at room temperature. *Appl. Phys. Lett.* **107**, 213301 (2015).
31. Nagata, R., Nakanotani, H., Potscavage, W. J. & Adachi, C. Exploiting Singlet Fission in Organic Light-Emitting Diodes. *Adv. Mater.* **30**, 1801484 (2018).
32. Pan, R. *et al.* Extraordinary magnetic field effects mediated by spin-pair interaction and electron mobility in thermally activated delayed fluorescence-based OLEDs with quantum-well structure. *J. Mater. Chem. C* **7**, 2421–2429 (2019).
33. Faulkner, L. R. & Bard, A. J. Electrogenerated chemiluminescence. IV. Magnetic field effects on the electrogenerated chemiluminescence of some anthracenes. *J. Am. Chem. Soc.* **91**, 209–210 (1969).
34. Pan, H. *et al.* Changing the Sign of Exchange Interaction in Radical Pairs to Tune Magnetic Field Effect on Electrogenerated Chemiluminescence. *J. Phys. Chem. C* **119**, 8089–8094 (2015).
35. Hattori, Y., Kusamoto, T. & Nishihara, H. Luminescence, Stability, and Proton Response of an Open-Shell (3,5-Dichloro-4-pyridyl)bis(2,4,6-trichlorophenyl)methyl Radical. *Angew. Chem. Int. Ed.* **53**, 11845–11848 (2014).
36. Kimura, S. *et al.* Magnetoluminescence in a Photostable, Brightly Luminescent Organic Radical in a Rigid Environment. *Angew. Chem. Int. Ed.* **57**, 12711–12715 (2018).
37. Kato, K., Kimura, S., Kusamoto, T., Nishihara, H. & Teki, Y. Luminescent Radical-Excimer: Excited-State Dynamics of Luminescent Radicals in Doped Host Crystals. *Angew. Chem. Int. Ed.* **58**, 2606–2611 (2019).
38. Kimura, S., Kimura, S., Nishihara, H. & Kusamoto, T. Excimer emission and magnetoluminescence of radical-based zinc(II) complexes doped in host crystals. *Chem. Commun.* **56**, 11195–11198 (2020).

39. Matsuoka, R., Kimura, S. & Kusamoto, T. Solid-State Room-Temperature Near-Infrared Photoluminescence of a Stable Organic Radical. *ChemPhotoChem* **5**, 669–673 (2021).
40. Kimura, S. *et al.* A ground-state-dominated magnetic field effect on the luminescence of stable organic radicals. *Chem. Sci.* **12**, 2025–2029 (2021).
41. Kusamoto, T. & Kimura, S. Photostable Luminescent Triarylmethyl Radicals and Their Metal Complexes: Photofunctions Unique to Open-shell Electronic States. *Chem. Lett.* **50**, 1445–1459 (2021).
42. Kimura, S., Matsuoka, R., Kimura, S., Nishihara, H. & Kusamoto, T. Radical-Based Coordination Polymers as a Platform for Magnetoluminescence. *J. Am. Chem. Soc.* **143**, 5610–5615 (2021).
43. Korenaga, T., Kawauchi, Y., Kosaki, T., Ema, T. & Sakai, T. Synthesis of a Molecular Tweezer Containing Pentafluorophenyl Groups and Investigation of the π–π Stacking Interaction for a Pentafluorophenyl Group in a Polar Organic Solvent. *Bull. Chem. Soc. Jpn.* **78**, 2175–2179 (2005).
44. Zimmerman, S. C., Zeng, Z., Wu, W. & Reichert, D. E. Synthesis and structure of molecular tweezers containing active site functionality. *J. Am. Chem. Soc.* **113**, 183–196 (1991).
45. Bleaney, B. & Bowers, K. D. Anomalous paramagnetism of copper acetate. *Proc. R. Soc. London. Ser. A. Math. Phys. Sci.* **214**, 451–465 (1952).

Acknowledgements

The present study was supported by JSPS KAKENHI Grant Numbers JP20H02759, JP22K05048, and JP21K14649, JST PRESTO Grant Number JPMJPR20L4, and research grants from Union Tool Scholarship Society and Uchida Energy Science Promotion Foundation. Emission spectra measurements under a magnetic field were performed at the High Field Laboratory for Superconducting Materials, Institute for Materials Research, Tohoku University (Project No: 20H0029 and 202012-HMKPD-0041). A part of this work was conducted in Institute for Molecular Science, supported by Advanced Research Infrastructure for Materials and Nanotechnology in Japan (JPMXP1222MS5001) of the Ministry of Education, Culture, Sport, Science and Technology (MEXT), Japan. The computation was performed using Research Center for Computational Science, Okazaki, Japan (Project: 22-IMS-C191, 21-IMS-C237).

Author contributions

T.K. and R.M. conceived the project. R.M. performed the synthetic experiments, X-ray crystallographic measurements, ESR measurements, DFT calculations, and photophysical measurements under ambient conditions. R.M., T.K., and S.K. performed photophysical measurements under a magnetic field. T.M. performed the quantum mechanical simulations. R.M., T.M., and T.K. discussed and proposed the MFE mechanisms. All the authors contributed in preparing the manuscript.

Competing interests

The authors declare no competing interests.